NANO LETTERS

2007
Vol. 7, No. 3
750−753

Raman Spectral Probing of Electronic Transition Energy E_{ii} Variation of Individual SWNTs under Torsional Strain

Bo Gao,[†] Xiaojie Duan,[†] Jin Zhang,*[,†] Tianjiao Wu,[†] Hyungbin Son,[‡] Jing Kong,[‡] and Zhongfan Liu*[,†]

Centre for Nanoscale Science and Technology (CNST), Beijing National Laboratory for Molecular Sciences (BNLMS), State Key Laboratory for Structural Chemistry of Unstable and Stable Species, Key Laboratory for the Physics and Chemistry of Nanodevices, College of Chemistry and Molecular Engineering, Peking University, Beijing 100871, P. R. China, and Department of Electrical Engineering and Computer Science, Massachusetts Institute of Technology, Cambridge, Massachusetts 02139

Received December 21, 2006; Revised Manuscript Received February 7, 2007

ABSTRACT

We present herein a rational approach to probe the torsional strain-induced electronic transition energy E_{ii} variation of individual SWNTs by resonant Raman spectroscopy (RRS). When a SWNT was manipulated by AFM tip through a path perpendicular to SWNT axis, both torsional and uniaxial strain would be introduced in SWNTs. Under the torsional strain, resonant Raman spectral mapping along a SWNT detected an M-shaped frequency (ω_{RBM}) and W-shaped intensity (I_S) variation of radial breathing mode (RBM) spectra, which were induced by the elastic retraction of the nanotubes in combination with the friction after the tip has been removed. The electronic transition energy E_{ii} variation along SWNTs by torsional strain follows a family pattern based on $q = (n - m)$ mod 3: for semiconducting SWNTs, E_{33}^S increases for $q = +1$, E_{33}^S decreases and E_{22}^S increases for $q = -1$, and for metallic SWNTs, E_{11}^M always increases.

Strain plays an important role in tuning material properties.[1,2] In single-walled carbon nanotubes (SWNTs), it can act as an important factor for modulating the band structure and properties.[3] Various schemes have been proposed or attempted to generate strains in carbon nanotubes and investigate their effects on properties of nanotubes such as creating radial compression in the tube by exerting hydrostatic pressure,[4] stretching the tube in composites[5] or by atomic force microscopy (AFM) manipulation,[6,7] and twisting the tube in a torsional pendulum.[8] The electronic band structures of carbon nanotubes can be modulated under these different strains. Theoretical calculations show that the effects of strains, including uniaxial strain and torsional strain, on electronic structures are related to $(n - m)$ mod 3.[3] Conductance measurement,[9] PL spectroscopy,[10] and resonant Raman spectroscopy (RRS)[11] have been used to measure the electronic band structures of SWNTs. Among these, RRS requires easier sample preparation and can characterize both metallic and semiconducting nanotubes.

Recently, using AFM manipulation, we have introduced torsional and uniaxial strain in individual SWNTs.[12] It is found that the two kinds of strain exhibit different effects on Raman spectra of SWNTs, for example, the torsional strain can make the frequency of radial breath mode (RBM) upshift while uniaxial strain downshifts the longitudinal mode of the G-band.[12] The effect of torsional strain on SWNTs' electronic transition energy E_{ii}, however, has not been investigated in detail.

In the present study, using resonant Raman spectroscopy, the effect of torsional strain on electronic band structures of different types of SWNTs was reported. It is found that, under torsional strain, the electronic transition energy E_{ii} variation of SWNTs follows a family pattern based on $q = (n - m)$ mod 3: for semiconducting SWNTs, E_{33}^S increases for $q = +1$, E_{33}^S decreases and E_{22}^S increases for $q = -1$, and for metallic SWNTs, E_{11}^M always increases.

As shown in Figure 1a, the SWNTs were grown on silicon substrate with a 1 μm thick oxide layer from ethanol chemical vapor deposition and had a typical length of several millimeters.[13] The AFM manipulation was performed along a predefined path perpendicular to the tube axis (Figure 1b). It can be seen that the SWNT has been dragged away from the manipulation point (insets of Figure 1b). During manipulation, SWNT would roll on the substrate due to the friction between them.[12] Raman spectra were collected by using micro-Raman spectroscopy ($\sim$1 μm spot size) with a

* Corresponding authors. E-mail: jinzhang@pku.edu.cn (J.Z.). Telephone and fax: 86-10-6275-7157.
[†] College of Chemistry and Molecular Engineering, Peking University.
[‡] Department of Electrical Engineering and Computer Science, Massachusetts Institute of Technology.

10.1021/nl063006g CCC: $37.00
Published on Web 02/28/2007

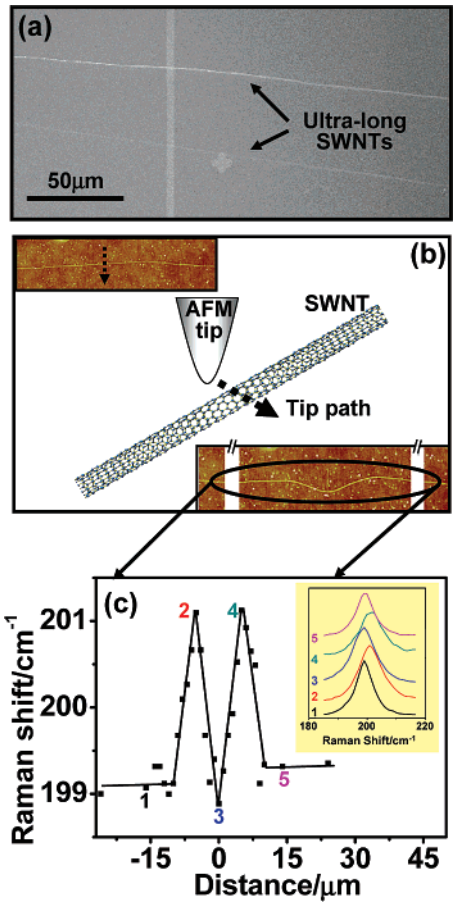

Figure 1. (a) Typical SEM image of ultralong SWNTs used for AFM manipulation. (b) Schematic illustrations of AFM manipulation on ultralong SWNTs. The upper left inset (10 μm × 2.5 μm) and lower right inset (60 μm × 2.5 μm) are AFM images of (14,2) SWNT before and after AFM manipulation. (c) RBM frequency profile of Stokes spectra along (14,2) SWNT axis after manipulation, which corresponds to the lower right inset of (b). The original ω_{RBM} before manipulation is at 198.9 cm^{-1}, and the manipulation point is at 0 μm. Inset shows the Stokes spectra of the indicated five points.

632.8 nm (1.959 eV) He−Ne laser, and the gratings were kept in the extended option. All the Raman spectra were fitted to Lorentzian peak shape to obtain the peak frequency and intensity and were calibrated by Rayleigh scattering.

A metallic SWNT with ω_{RBM} at 198.9 cm^{-1}, assigned as (14,2), was manipulated (insets of Figure 1b) and the typical RBM spectra were shown in the inset of Figure 1c, which can be normally used to estimate chiral indices (n,m) and E_{ii} values.[11,14] The continuous ω_{RBM} upshift from 198.9 to 201.1 cm^{-1} showed an M shape along the SWNT axis (Figure 1c) where the manipulation point was at zero. This upshift was caused by the torsional strain. The triangular profile was induced by the elastic retraction of the nanotubes in combination with the friction after the tip has been removed.[12] The torsional strain also caused dramatic change of the intensity of RBM spectra. As seen from Figure 2a, I_S forms a W-shaped and I_{AS}/I_S forms an M-shaped profile along the nanotube in the torsional region, indicating a decrease of I_S and an increase of I_{AS}/I_S induced by torsional strain respectively.

It has been commonly accepted that the intensity of resonant Raman spectra is sensitive to the E_{ii} of SWNTs.[15] Hence the I_S variation reflects the modulation of E_{ii} of SWNTs by torsional strain. The I_{AS}/I_S variation of RBM spectra can be quantitatively analyzed by resonant Raman theory,[16] which satisfies the following equation

$$\frac{I_{AS}}{I_S} = \frac{|(E_{laser} - E_{ii} - i\Gamma)(E_{laser} - E_{ph} - E_{ii} - i\Gamma)|^2}{|(E_{laser} - E_{ii} - i\Gamma)(E_{laser} + E_{ph} - E_{ii} - i\Gamma)|^2} \times \exp\left(-\frac{E_{ph}}{k_B T}\right)$$

It can be seen that, for a fixed laser energy E_{laser} and phonon energy E_{ph}, I_{AS}/I_S is E_{ii} dependent. If the inverse scattering lifetime Γ is assumed to be constant, the E_{ii} can be estimated from I_{AS}/I_S using the above equation (Figure 2b). As shown in Figure 2c, based on data from −8 to −5 μm, a theoretical fitting was performed on the experimental data of I_S and I_{AS}/I_S and an optimal value of Γ, 20 meV for (14,2) SWNT, was obtained. Such Γ is comparable with the calculated values of most isolated tubes.[17] By taking Γ = 20 meV, E_{ph} = 25 meV (ω_{RBM} = 198.9 cm^{-1}), all the E_{11}^M along SWNT axis was calculated and shown in Figure 2d. With the continuous increase of strain σ from −8 to −5 μm, E_{11}^M increases continuously from 1.951 to 1.967 eV (about 16 meV). That is, for metallic (14,2) SWNT, $dE_{11}^M/d\sigma$ is positive. The variation of E_{11}^M might be originated from the shift of Fermi wave vector $\mathbf{k}_F$ away from Brillouin zone vertices induced by strains.

For another semiconducting (13,11) SWNT with ω_{RBM} at 148.5 cm^{-1}, after manipulation, Raman spectra also varied due to torsional strain, which is similar to (14,2) SWNT. In strained region, I_S decreased and formed a W shape along the SWNT axis; accordingly, I_{AS}/I_S increased and formed an M shape (Figure 3a). The optimal Γ value of 30 meV was estimated by theoretically fitting experimental I_S and I_{AS}/I_S data (Inset of Figure 3b). Using the equation above, the E_{33}^S along the SWNT axis were obtained as shown in Figure 3b. It can be observed that, as torsional strain σ continuously increased from −15 to −8 μm, E_{33}^S decreased continuously from 1.865 to 1.823 eV. Hence, for semiconducting (13,11) SWNT, $dE_{33}^S/d\sigma$ is negative, which is contrary to the metallic (14,2) SWNT.

As listed in Table 1, we have collected the data of 10 individual ultralong SWNTs, including six semiconducting tubes and four metallic tubes. All the ω_{RBM} were collected before manipulation and calibrated by Rayleigh scattering. Chiral indices (n,m) were assigned based on ω_{RBM} and I_{AS}/I_S.[11,14] The Γ values were estimated by theoretically fitting experimental I_S and I_{AS}/I_S data. Then E_{ii} and ΔE_{ii} were calculated using the above equation. It is found that, after manipulation, the ω_{RBM} of all SWNTs upshifted due to torsional strain and the variation of E_{ii} induced by σ is related to q. Under torsional strain, for semiconducting SWNTs, E_{33}^S increases for q = +1, E_{33}^S decreases and E_{22}^S increases for q = −1, and for metallic SWNTs, E_{11}^M always increases. It has been reported theoretically[3] that the torsional strain-

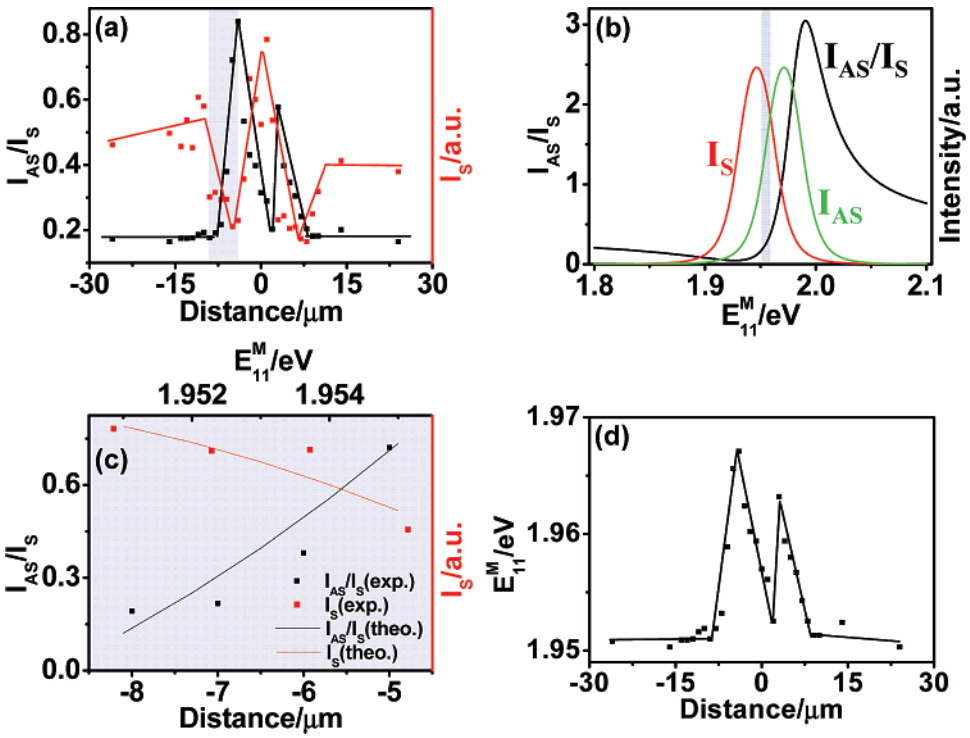

Figure 2. (a) I_S (red dots and lines) and I_{AS}/I_S (black dots and lines) profiles of RBM spectra along (14,2) SWNT axis after manipulation. Dots are experiment data and lines are linear curve-fitted results. The blue-shaded region is used to estimate Γ as shown in (c). (b) Normalized intensity of resonant Raman spectra for both the Stokes (red line) and anti-Stokes (green line) Raman processes as a function of E_{ii} under a fixed E_{laser} (1.959 eV). The black line is I_{AS}/I_S corrected by the Bose−Einstein thermal factor. (c) Fitting between experimental I_S and I_{AS}/I_S data (dots) and theoretical calculation (lines). The obtained Γ value is 20 meV. The experimental data are from blue-shaded region of (a), from −8 to −5 μm. (d) E_{11}^M along SWNT axis after manipulation. Dots are values calculated using the equation in text and lines are linear curve-fitted results.

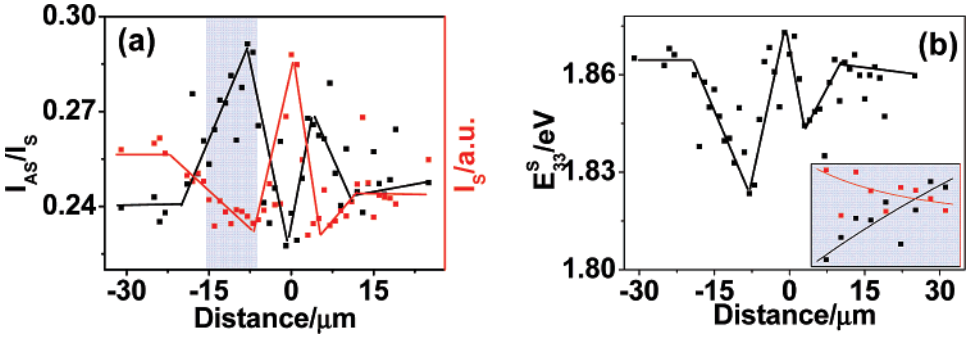

Figure 3. (a) I_S (red dots and lines) and I_{AS}/I_S (black dots and lines) profiles of RBM spectra along (13,11) SWNT axis after manipulation. Dots are experiment data and lines are linear curve-fitted results. The blue-shaded region is used to estimate Γ as shown in inset of (b). (b) E_{33}^S along SWNT axis after manipulation. Dots are values calculated using the equation in text and lines are linear curve-fitted results. Inset: the Γ value of 30 meV was obtained by fitting between experimental I_S and I_{AS}/I_S data and theoretical calculation as done in Figure 2c. The experimental data are from blue-shaded region of (b), from −15 to −8 μm.

induced variation of E_{ii} is related to the sign of q and the van Hove singularity index i (1,2,3,...). The relative positions of semiconducting SWNTs with $q = +1$ and $q = -1$ in $\mathbf{k}$ space are opposite relative to the Brillouin zone vertices. Under torsional strain, perturbations to the Fermi wave vector $\mathbf{k}_F$ act in opposite directions and consequently cause shifts of E_{ii} in different directions. E_{22}^S and E_{33}^S are generated where two cutting lines on the two sides of Brillouin zone vertices cross with π and π^* electronic states so that they have opposite responses under torsional strain. For metallic SWNTs, $dE_{11}^M/d\sigma$ is always positive. This is because the resonance with the higher energy component of E_{11}^M has a much lower intensity than that of the lower energy component, and only the lower energy component of E_{11}^M can be detected by RRS.[18]

It should be noted that most calculated E_{ii} profiles showed asymmetrical behavior at the two sides of the manipulation points. In our system, for chiral SWNTs, the two parts beside the manipulation points will be twisted in opposite direction; this may cause some difference in the E_{ii} variation and result in the asymmetrical E_{ii} profiles.

We also found in our experiment, as shown in Table 1, after breaking, the maximal upshifts of ω_{RBM}[19] ranged from 0.55 to 2.13 cm^{-1} and the maximal variations of E_{ii} were

Table 1. Results of 10 Manipulated Ultralong SWNTs[a]

ω_{RBM} (cm^{-1})	(n,m)	Γ (meV)	$\Delta\omega_{RBM}^{max}$ (cm^{-1})	ΔE_{ii}^{max} (meV)	$dE_{ii}/d\sigma$	($n - m$) mod 3
141.4	(15,10)	40	+1.55	−10.1	$dE_{33}^{S}/d\sigma < 0$	−1
148.5	(13,11)	30	+2.13	−39.1		
160.6	(12,10)	30	+1.47	−9.0		
155.9	(16,6)	30	+0.58	+1.0	$dE_{33}^{S}/d\sigma > 0$	+1
159.4	(13,9)	30	+1.13	+4.5		
285.8	(7,5)	20	+1.34	−	$dE_{22}^{S}/d\sigma > 0$	−1
177.1	(14,5)	30	+0.90	+4.9	$dE_{11}^{M}/d\sigma > 0$	0
198.9	(14,2)	20	+2.10	+15.8		
211.9	(11,5)	30	+1.40	−		
218.6	(13,1)	30	+0.55	+6.5		

[a] All the ω_{RBM} were collected before manipulation and calibrated by Rayleigh scattering. Chiral indices (n,m) are assigned based on ω_{RBM} and I_{AS}/I_S. The inverse scattering lifetime Γ are obtained by fitting experimental I_S and I_{AS}/I_S data to theoretical calculation, as done in Figure 2c. $\Delta\omega_{RBM}^{max}$ and ΔE_{ii}^{max} are respectively the maximum variation of ω_{RBM} and E_{ii} after SWNTs were broken. σ is the torsional strain. "−" means that anti-Stokes spectra were too weak and were not completely collected.

between 1.0 and 39.1 meV, which has some relation to the chiral indices (n,m). Moreover, the ω_{RBM} of SWNTs close to armchair upshifted more than those close to zigzag. This also applied to the variation of E_{ii}. It is possible that SWNTs close to armchair are more sensitive to torsional strain than those close to zigzag.[3] Comparing semiconducting SWNTs with $q = -1$ to $+1$, the upshift of ω_{RBM} and the variation of E_{33}^{S} are more obvious for $q = -1$. We can infer that, for SWNTs with $q = -1$, torsional strain can result in larger phonon variation and E_{33}^{S} variation for the same shift of $\mathbf{k}_F$. It could be understood as following: near the K point at the corner of hexagonal Brillouin zone, due to trigonal warping effect, equi-energy contours along $\Gamma-K$ line at the inner of Brillouin zone are denser than that along $K-M$ line at the outer.[20] That is, E_{ii} varies more quickly at the inner than that at the outer. The third nearest cutting line of SWNTs with $q = -1$ is at the inner of Brillouin zone, and $q = +1$ at the outer. Thus, under equal torsional strain, E_{33}^{S} of SWNTs with $q = -1$ varies more quickly. The detailed study is underway.

In summary, this work gives the first systematically experimental study of the torsional strain effect on the electronic band structure of SWNTs. It is found that, under torsional strain, the electronic transition energy E_{ii} variation of SWNTs follows a family pattern based on $q = (n - m)$ mod 3: for semiconducting SWNTs, E_{33}^{S} increases for $q = +1$, E_{33}^{S} decreases and E_{22}^{S} increases for $q = -1$, and for metallic SWNTs, E_{11}^{M} always increases. The family pattern can be of great use to determine the chiral indices (n,m). Also, SWNTs with continuous variation of E_{ii} along its axis might show potential applications in nanoelectromechanical system.

Acknowledgment. This work was supported by NSFC (20573002, 20673004, 50521201) and MOST (2006CB932701, 2006CB932403). H. Son and J. Kong gratefully acknowledge support from the Intel Higher Education Program.

Supporting Information Available: Chiral indices (n,m) assignments of metallic and semiconducting SWNTs. This material is available free of charge via the Internet at http://pubs.acs.org.

References

(1) Takagi, S.; Mizuno, T.; Sugiyama, N.; Tezuka, T.; Kurobe *IEICE Trans. Electron.* **2001**, *E84C*, 1043.
(2) Johnson, H. T.; Freund, L. B. *Int. J. Solids Struct.* **2001**, *38*, 1045.
(3) Yang, L.; Han, J. *Phys. Rev. Lett.* **2000**, *85*, 154.
(4) Venkateswaran, U. D.; Rao, A. M.; Richter, E.; Menon, M.; Rinzler, A.; Smalley, R. E.; Eklund, P. C. *Phys. Rev. B* **1999**, *59*, 10928.
(5) Cooper, C. A.; Young, R. J.; Halsall, M. *Composites, Part A* **2001**, *32*, 401.
(6) Cronin, S. B.; Swan, A. K.; Unlu, M. S.; Goldberg, B. B.; Dresselhaus, M. S.; Tinkham, M. *Phys. Rev. Lett.* **2004**, *93*, 167401.
(7) Minot, E. D.; Yaish, Y.; Sazonova, V.; Park, J. Y.; Brink, M.; McEuen, P. L. *Phys. Rev. Lett.* **2003**, *90*, 156401.
(8) Meyer, J. C.; Paillet, M.; Roth, S. *Science* **2005**, *309*, 1539.
(9) Odom, T. W.; Huang, J. L.; Kim, P.; Lieber, C. M. *Nature* **1998**, *391*, 62.
(10) O'Connell, M. J.; Bachilo, S. M.; Huffman, C. B.; Moore, V. C.; Strano, M. S.; Haroz, E. H.; Rialon, K. L.; Boul, P. J.; Noon, W. H.; Kittrell, C.; Ma, J. P.; Hauge, R. H.; Weisman, R. B.; Smalley, R. E. *Science* **2002**, *297*, 593.
(11) Maultzsch, J.; Telg, H.; Reich, S.; Thomsen, C. *Phys. Rev. B* **2005**, *72*, 205438.
(12) Duan, X. J.; Son, H. B.; Zhang, J.; Gao, B.; Wu, T. J.; Liu, Z. F.; Kong, J. Submitted.
(13) Zhang, Y. Y.; Zhang, J.; Son, H. B.; Kong, J.; Liu, Z. F. *J. Am. Chem. Soc.* **2005**, *127*, 17156.
(14) Strano, M. S. *J. Am. Chem. Soc.* **2003**, *125*, 16148.
(15) Pimenta, M. A.; Marucci, A.; Brown, S. D. M.; Matthews, M. J.; Rao, A. M.; Eklund, P. C.; Smalley, R. E.; Dresselhaus, G.; Dresselhaus, M. S. *J. Mater. Res.* **1998**, *13*, 2396.
(16) Souza, A. G.; Jorio, A.; Hafner, J. H.; Lieber, C. M.; Saito, R.; Pimenta, M. A.; Dresselhaus, G.; Dresselhaus, M. S. *Phys. Rev. B* **2001**, *63*, 241404.
(17) Park, J. S.; Oyama, Y.; Saito, R.; Izumida, W.; Jiang, J.; Sato, K.; Fantini, C.; Jorio, A.; Dresselhaus, G.; Dresselhaus, M. S. *Phys. Rev. B* **2006**, *74*, 165414.
(18) Souza, A. G.; Kobayashi, N.; Jiang, J.; Gruneis, A.; Saito, R.; Cronin, S. B.; Mendes, J.; Samsonidze, G. G.; Dresselhaus, G. G.; Dresselhaus, M. S. *Phys. Rev. Lett.* **2005**, *95*, 217403.
(19) In our experiment, Raman spectra varies continuously and linearly along ultralong SWNTs. By curve-fitting, the equipment errors could be greatly decreased and the precision would be much better than typical resolution of Raman spectroscopy (about 1 cm^{-1}).
(20) Saito, R.; Dresselhaus, G.; Dresselhaus, M. S. *Phys. Rev. B* **2000**, *61*, 2981.

NL063006G